Supporting Information for: The different facets of ice have different hydrophilicities: Friction at water / ice-I_h interfaces

Patrick B. Louden * **and J. Daniel Gezelter** *

*Department of Chemistry and Biochemistry, University of Notre Dame, Notre Dame, IN 46556

Submitted to Proceedings of the National Academy of Sciences of the United States of America

Overview

The supporting information contains further details about the model construction, analysis methods, and supplies figures that support the data presented in the main text.

Construction of the Ice / Water interfaces

Ice I_h crystallizes in the hexagonal space group $P6_3/mmc$, and common ice crystals form hexagonal plates with the basal face $\{0001\}$ forming the top and bottom of each plate, and the prismatic facet $\{10\bar{1}0\}$ forming the sides. In extreme temperatures or low water saturation conditions, ice crystals can easily form as hollow columns, needles and dendrites. These are structures that expose other crystalline facets of the ice to the surroundings. Among the more common facets are the secondary prism, $\{11\bar{2}0\}$, and pyramidal, $\{20\bar{2}1\}$, faces.

We found it most useful to work with proton-ordered, zero-dipole crystals that expose strips of dangling H-atoms and lone pairs.(**?**) Our structures were created starting from Structure 6 of Hirsch and Ojamäe's set of orthorhombic representations for ice-I_h (**?**). This crystal structure was cleaved along the four different facets. The exposed face was reoriented normal to the z-axis of the simulation cell, and the structures were and extended to form large exposed facets in rectangular box geometries. Liquid water boxes were created with identical dimensions (in x and y) as the ice, with a z dimension of three times that of the ice block, and a density corresponding to 1 g / cm^3. Each of the ice slabs and water boxes were independently equilibrated at a pressure of 1 atm, and the resulting systems were merged by carving out any liquid water molecules within 3 Å of any atoms in the ice slabs. Each of the combined ice/water systems were then equilibrated at 225K, which is the liquid-ice coexistence temperature for SPC/E water (**?**). Reference **?** contains a more detailed explanation of the construction of similar ice/water interfaces. The resulting dimensions as well as the number of ice and liquid water molecules contained in each of these systems are shown in Table S1.

A second method for computing contact angles

In addition to the spherical cap method outlined in the main text, a second method for obtaining the contact angle was described by Ruijter, Blake, and Coninck (**?**). This method uses a cylindrical averaging of the droplet's density profile. A threshold density of 0.5 g cm^{-3} is used to estimate the location of the edge of the droplet. The r and z-dependence of the droplet's edge is then fit to a circle, and the contact angle is computed from the intersection of the fit circle with the z-axis location of the solid surface. Again, for each stored configuration, the density profile in a set of annular shells was computed. Due to large density fluctuations close to the ice, all shells located within 2 Å of the ice surface were left out of the circular fits. The height of the solid surface (z_{suface}) along with the best fitting origin (z_{droplet}) and radius (r_{droplet}) of the droplet can then be used to compute the contact angle,

$$\theta = 90 + \frac{180}{\pi} \sin^{-1}\left(\frac{z_{\mathrm{droplet}} - z_{\mathrm{surface}}}{r_{\mathrm{droplet}}}\right). \qquad [\mathbf{S1}]$$

Determining interfacial widths using structural information

To determine the structural widths of the interfaces under shear, each of the systems was divided into 100 bins along the z-dimension, and the local tetrahedral order parameter (Eq. 5 in Reference **?**) was time-averaged in each bin for the duration of the shearing simulation. The spatial dependence of this order parameter, $q(z)$, is the tetrahedrality profile of the interface. The lower panels in figures S2-S5 in the SI show tetrahedrality profiles (in circles) for each of the four interfaces. The $q(z)$ function has a range of $(0, 1)$, where a value of unity indicates a perfectly tetrahedral environment. The $q(z)$ for the bulk liquid was found to be ≈ 0.77, while values of ≈ 0.92 were more common in the ice. The tetrahedrality profiles were fit using a hyperbolic tangent function (see Eq. 6 in Reference **?**) designed to smoothly fit the bulk to ice transition while accounting for the weak thermal gradient. In panels b and c of the same figures, the resulting thermal and velocity gradients from an imposed kinetic energy and momentum fluxes can be seen. The vertical dotted lines traversing these figures indicate the midpoints of the interfaces as determined by the tetrahedrality profiles.

Determining interfacial widths using dynamic information

To determine the dynamic widths of the interfaces under shear, each of the systems was divided into bins along the z-dimension (≈ 3 Å wide) and $C_2(z, t)$ was computed using only those molecules that were in the bin at the initial time.

Reserved for Publication Footnotes

The time-dependence was fit to a triexponential decay, with three time constants: τ_{short}, measuring the librational motion of the water molecules, τ_{middle}, measuring the timescale for breaking and making of hydrogen bonds, and τ_{long}, corresponding to the translational motion of the water molecules. An additional constant was introduced in the fits to describe molecules in the crystal which do not experience long-time orientational decay.

In Figures S6-S9 in the supporting information, the z-coordinate profiles for the three decay constants, τ_{short}, τ_{middle}, and τ_{long} for the different interfaces are shown. (Figures S6 & S7 are new results, and Figures S8 & S9 are updated plots from Ref **?** .) In the liquid regions of all four interfaces, we observe τ_{middle} and τ_{long} to have approximately consistent values of $3-6$ ps and $30-40$ ps, respectively. Both of these times increase in value approaching the interface. Approaching the interface, we also observe that τ_{short} decreases from its liquid-state value of $72-76$ fs. The approximate values for the decay constants and the trends approaching the interface match those reported previously for the basal and prismatic interfaces.

We have estimated the dynamic interfacial width $d_{\rm dyn}$ by fitting the profiles of all the three orientational time constants with an exponential decay to the bulk-liquid behavior,

$$\tau(z) \approx \tau_{liquid} + (\tau_{wall} - \tau_{liquid}) e^{-(z-z_{wall})/d_{\rm dyn}} \qquad [\mathbf{S2}]$$

where τ_{liquid} and τ_{wall} are the liquid and projected wall values of the decay constants, z_{wall} is the location of the interface, as measured by the structural order parameter. These values are shown in table **??**. Because the bins must be quite wide to obtain reasonable profiles of $C_2(z,t)$, the error estimates for the dynamic widths of the interface are significantly larger than for the structural widths. However, all four interfaces exhibit dynamic widths that are significantly below 1 nm, and are in reasonable agreement with the structural width above.

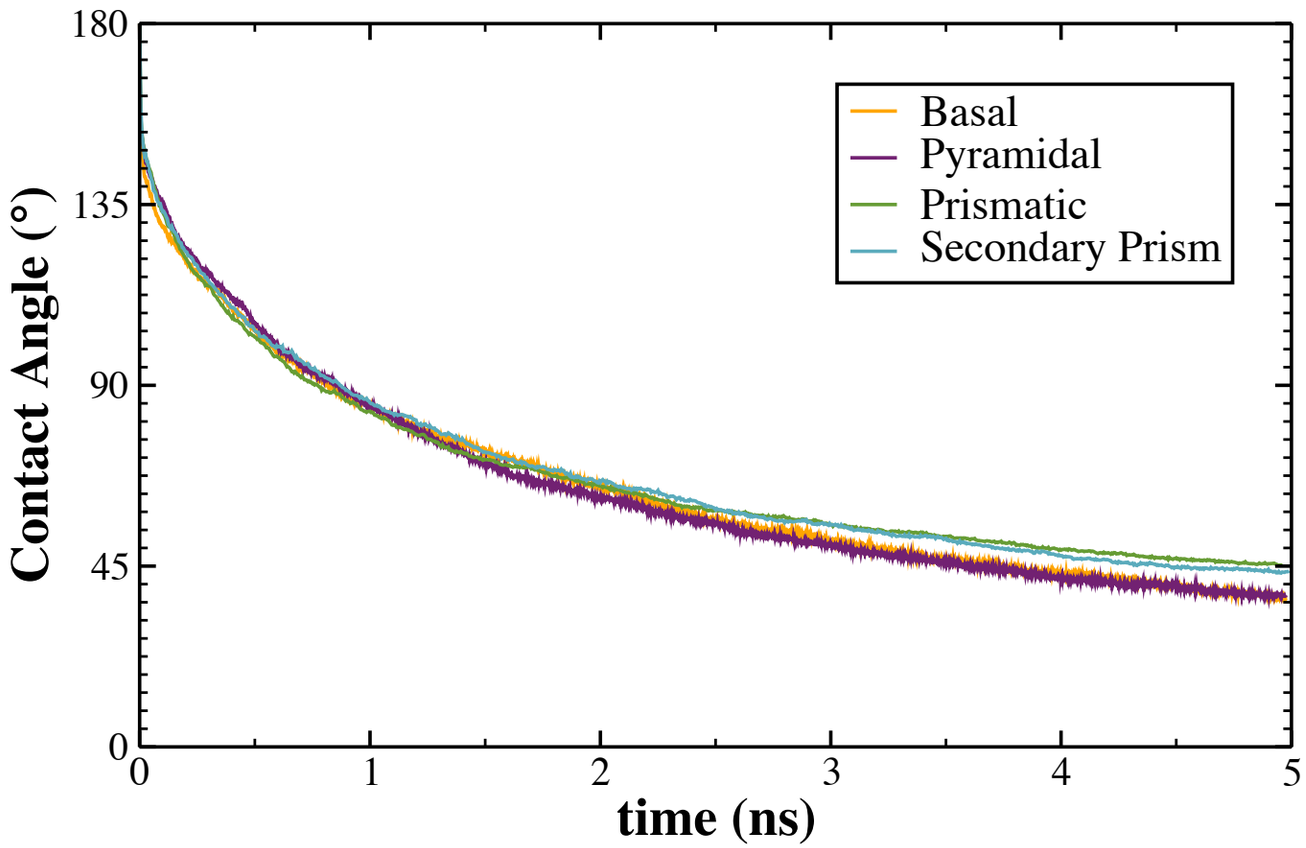

Fig. S1. The dynamic contact angle of a droplet after approaching each of the four ice facets. The decay to an equilibrium contact angle displays similar dynamics. Although all the surfaces are hydrophilic, the long-time behavior stabilizes to significantly flatter droplets for the basal and pyramidal facets. This suggests a difference in hydrophilicity for these facets compared with the two prismatic facets.

Table S1. Sizes of the droplet and shearing simulations. Cell dimensions are measured in Å.

Interface	Droplet				Shearing				
	N_{ice}	N_{droplet}	L_x	L_y	N_{ice}	N_{liquid}	L_x	L_y	L_z
Basal $\{0001\}$	12960	2048	134.70	140.04	900	1846	23.87	35.83	98.64
Pyramidal $\{20\bar{2}1\}$	11136	2048	143.75	121.41	1216	2203	37.47	29.50	93.02
Prismatic $\{10\bar{1}0\}$	9900	2048	110.04	115.00	3000	5464	35.95	35.65	205.77
Secondary Prism $\{11\bar{2}0\}$	11520	2048	146.72	124.48	3840	8176	71.87	31.66	161.55

References

1. Buch V, Groenzin H, Li I, Shultz MJ, Tosatti E (2008) Proton order in the ice crystal surface. *Proceedings of the National Academy of Sciences* 105(16):5969–5974.
2. Hirsch TK, Ojamäe L (2004) Quantum-chemical and force-field investigations of ice ih: Computation of proton-ordered structures and prediction of their lattice energies. *The Journal of Physical Chemistry B* 108(40):15856–15864.
3. Bryk T, Haymet ADJ (2002) Ice 1h/water interface of the spc/e model: Molecular dynamics simulations of the equilibrium basal and prism interfaces. *The Journal of Chemical Physics* 117(22):10258–10268.
4. Louden PB, Gezelter JD (2013) Simulations of solid-liquid friction at ice-ih/water interfaces. *The Journal of Chemical Physics* 139(19):–.
5. de Ruijter MJ, Blake TD, Coninck JD (1999) Dynamic wetting studied by molecular modeling simulations of droplet spreading. *Langmuir* 15:7836–7847.

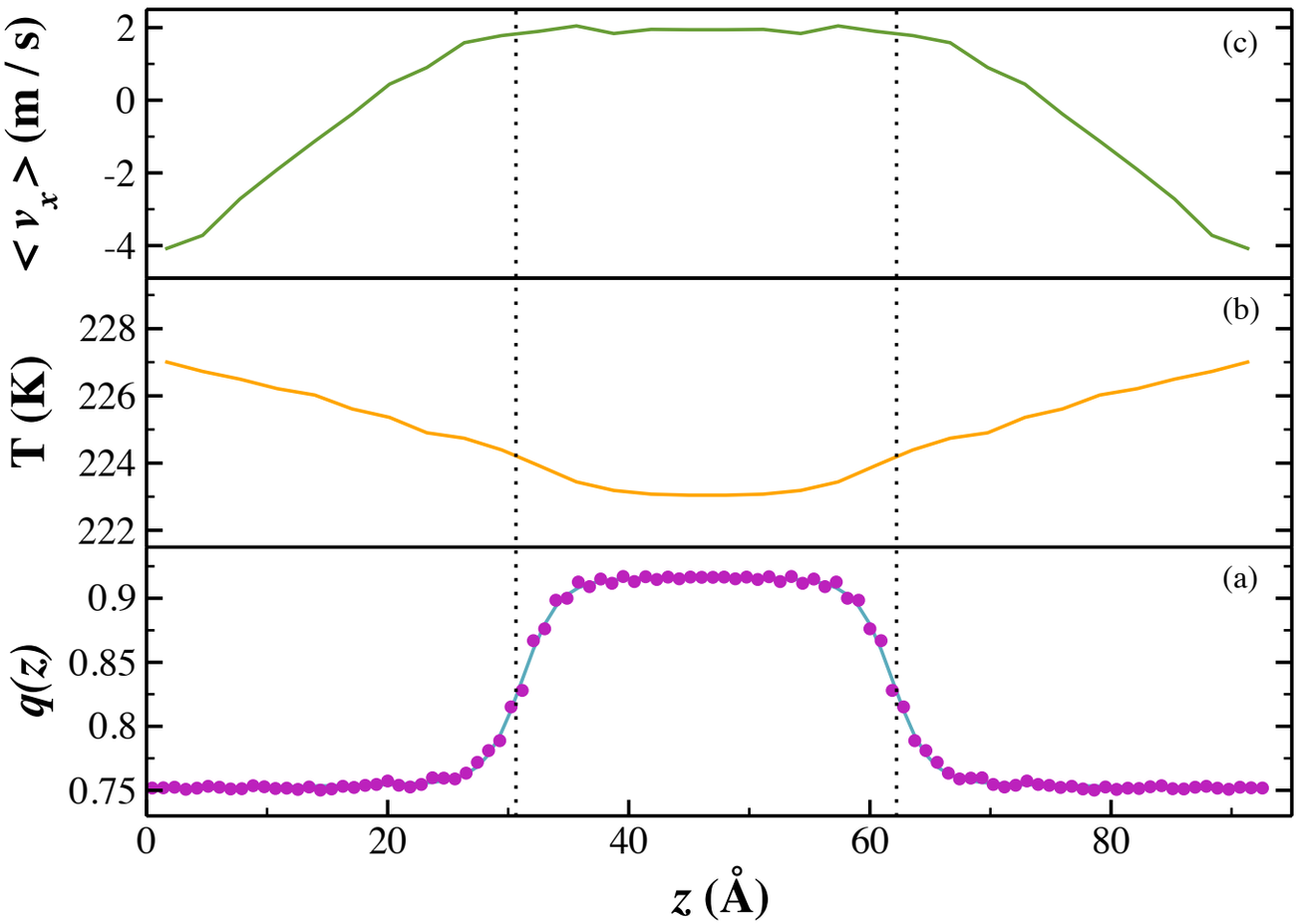

Fig. S2. Properties of the pyramidal interface being sheared through water at 3.8 ms^{-1}. Lower panel: the local tetrahedral order parameter, $q(z)$, (circles) and the hyperbolic tangent fit (turquoise line). Middle panel: the imposed thermal gradient required to maintain a fixed interfacial temperature of 225 K. Upper panel: the transverse velocity gradient that develops in response to an imposed momentum flux. The vertical dotted lines indicate the locations of the midpoints of the two interfaces.

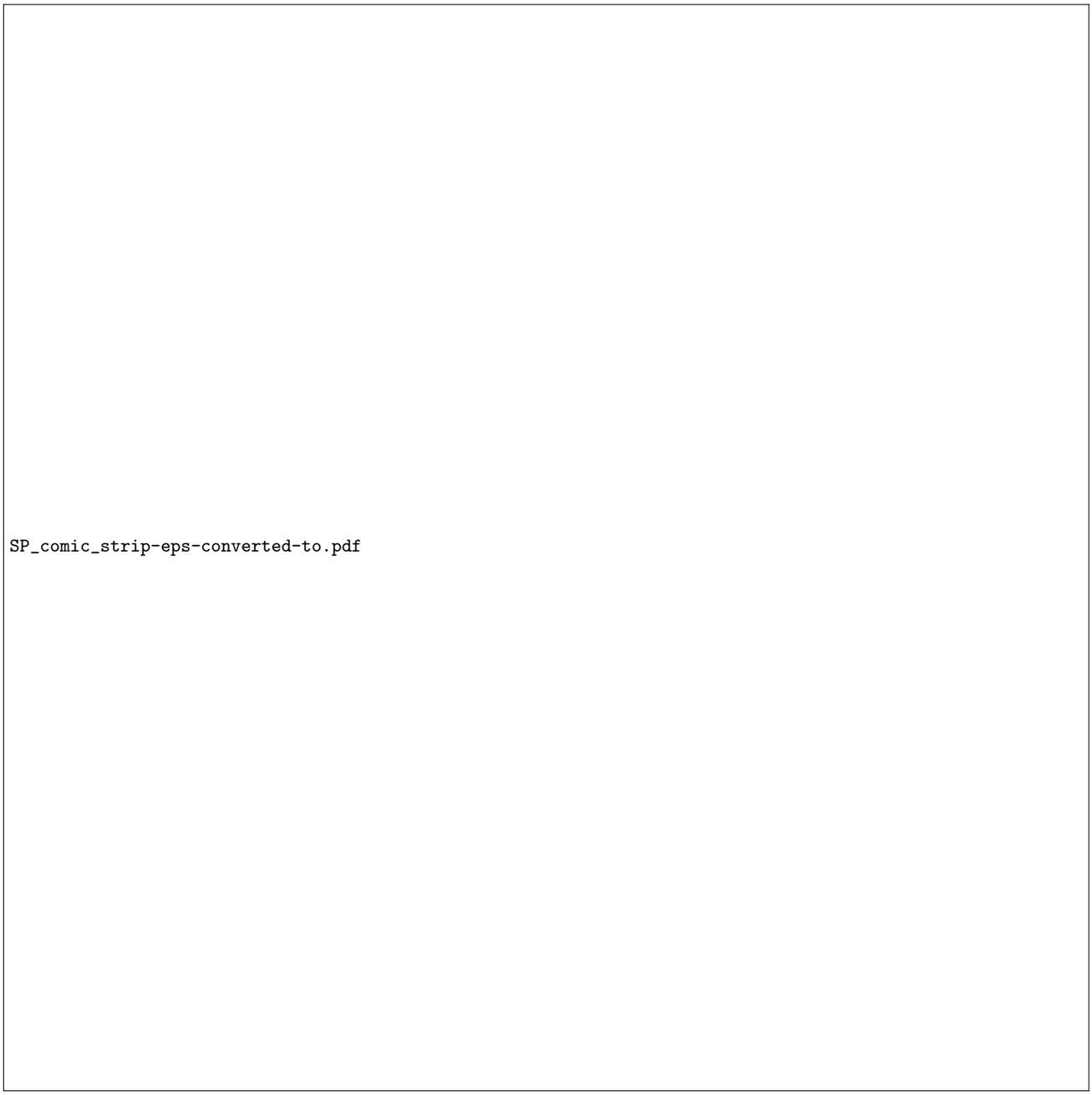

Fig. S3. The secondary prism interface with a shear rate of 3.5 ms^{-1}. Panel descriptions match those in figure S2.

Fig. S4. The basal interface with a shear rate of 1.3 ms^{-1}. Panel descriptions match those in figure S2.

Fig. S5. The prismatic interface with a shear rate of 2 ms^{-1}. Panel descriptions match those in figure S2.

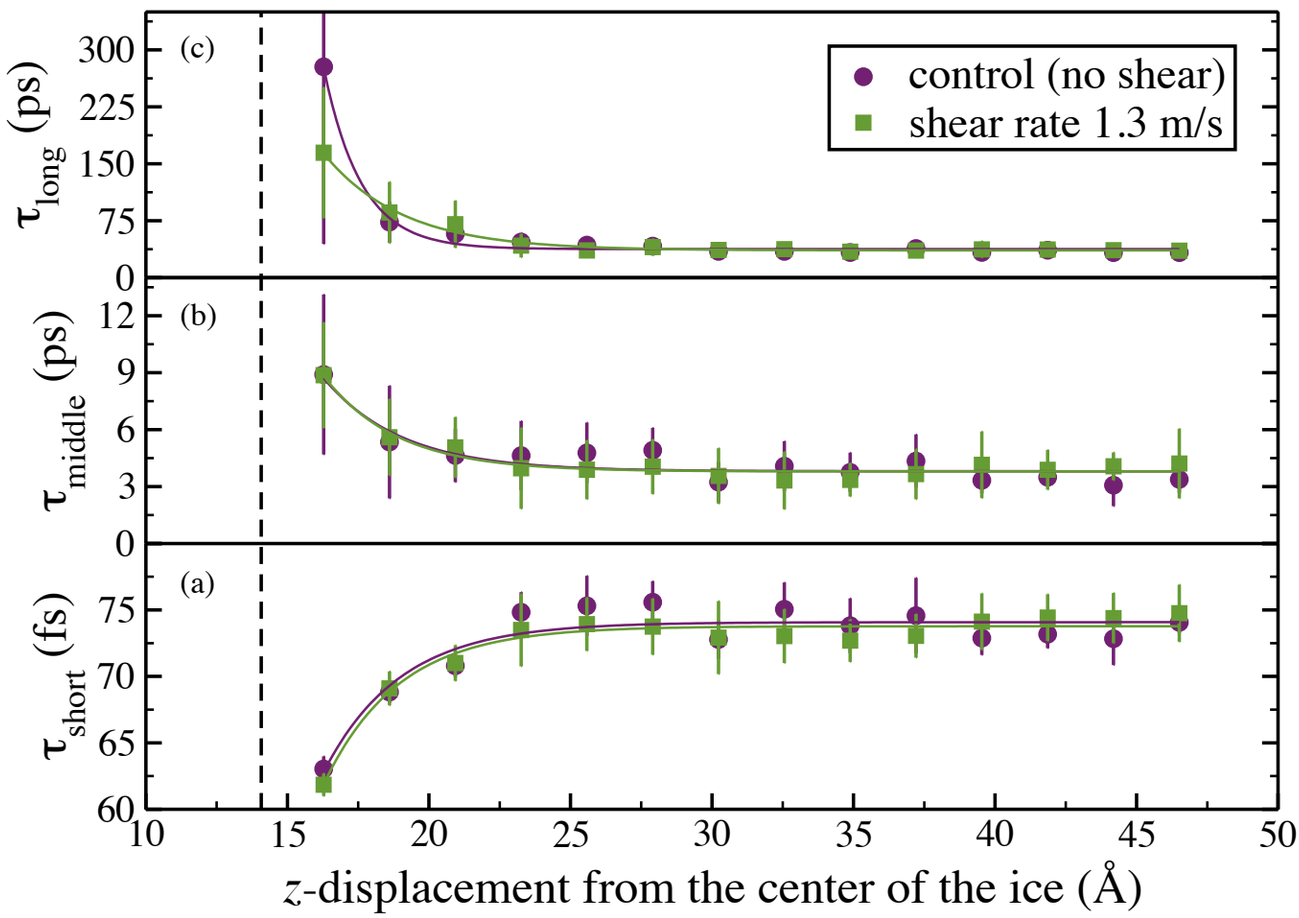

Fig. S6. The three decay constants of the orientational time correlation function, $C_2(z,t)$, for water as a function of distance from the center of the ice slab. The vertical dashed line indicates the edge of the pyramidal ice slab determined by the local order tetrahedral parameter. The control (circles) and sheared (squares) simulations were fit using shifted-exponential decay (see Eq. 9 in Ref. **?**).

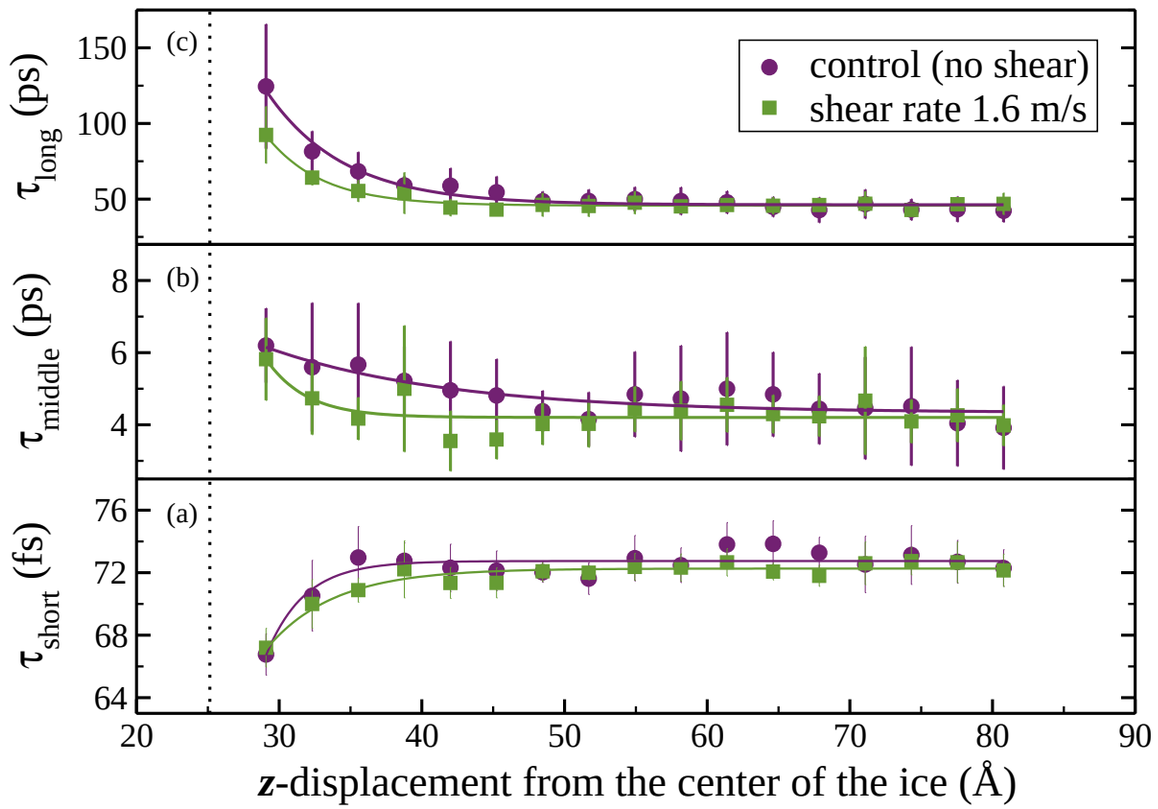

Fig. S7. Decay constants for $C_2(z,t)$ at the secondary prism face. Panel descriptions match those in S6.

Fig. S8. Decay constants for $C_2(z,t)$ at the basal face. Panel descriptions match those in S6.

Fig. S9. Decay constants for $C_2(z,t)$ at the prismatic face. Panel descriptions match those in S6.